

The East Asian Summer Monsoon in pacemaker experiments driven by ENSO

Hui Ding · Richard J. Greatbatch · Jian Lu · Ben Cash

Received: 28 August 2014 / Accepted: 21 November 2014 / Published online: 16 December 2014
© Springer-Verlag Berlin Heidelberg (outside the USA) 2014

Abstract The variability of the East Asian summer monsoon (EASM) is studied using a pacemaker technique driven by ENSO in an atmospheric general circulation model (AGCM) coupled to a slab mixed layer model. In the pacemaker experiments, sea surface temperature (SST) is constrained to observations in the eastern equatorial Pacific through a *q-flux* that measures the contribution of ocean dynamics to SST variability, while the AGCM is coupled to the slab model. An ensemble of pacemaker experiments is analyzed using a multivariate EOF analysis to identify the two major modes of variability of the EASM. The results show that the pacemaker experiments simulate a substantial amount (around 45 %) of the variability of the first mode (the Pacific-Japan pattern) in ERA40 from 1979 to 1999. Different from previous work, the pacemaker experiments also simulate a large part (25 %) of the variability of the second mode, related to rainfall variability over northern China. Furthermore, we find that the lower (850 hPa) and the upper

(200 hPa) tropospheric circulation of the first mode display the same degree of reproducibility whereas only the lower part of the second mode is reproducible. The basis for the success of the pacemaker experiments is the ability of the experiments to reproduce the observed relationship between El Niño Southern Oscillation (ENSO) and the EASM.

Keywords East Asian Summer Monsoon · Pacemaker · ENSO

1 Introduction

The East Asian Summer Monsoon (EASM) is an important component of the Asian-Australian monsoon system (Wang, 2006). The EASM brings summer rainfall to China, Japan, and Korea from the tropical Indian and Pacific Oceans and sustains about one fifth of the human population. Fluctuations of the EASM have a profound impact on East Asia (e.g., Rodwell and Hoskins 2001). Thus, it is of great socioeconomic interest to investigate the variability of the EASM.

Numerous studies have reported the influence of ENSO (Philander 1990) on the western North Pacific and East Asian summer climate (e.g., Zhang et al. 1999; Wang et al. 2000; Wu et al. 2003; Wu and Kirtman 2004; Lu et al. 2006; Li et al. 2007; Wang et al. 2008; Sun et al. 2010). The physical process that transfers the ENSO signal to the western North Pacific and East Asia has been extensively studied (e.g., Wang et al. 2000; Wang and Zhang 2002; Lau and Nath 2006). Recently, some studies found that the Indian Ocean capacity effect has a role to play in order to prolong the influence of ENSO from winter to the following summer (e.g., Xie et al. 2009, 2010). The influence of ENSO provides a physical foundation for predictability of the lower

Responsible Editor: Jinyu Sheng

This article is part of the Topical Collection on *Atmosphere and Ocean Dynamics: A Scientific Workshop to Celebrate Professor Dr. Richard Greatbatch's 60th Birthday, Liverpool, UK, 10-11 April 2014*

H. Ding (✉) · R. J. Greatbatch
GEOMAR Helmholtz Centre for Ocean Research Kiel,
Kiel, Germany
e-mail: hding@geomar.de

J. Lu
Pacific Northwest National Laboratory, 902 Battelle Boulevard,
Richland, WA USA

B. Cash
Center for Ocean-Land-Atmosphere Studies, Institute of Global
Environment and Society, Calverton, Maryland, USA

tropospheric summer circulation over the western North Pacific and East Asia (Li et al. 2012, 2014). Nevertheless, potential predictability of the EASM is thought to be low, given the claim that the variability of the EASM is dominated by atmospheric internal variability (e.g., Lu et al. 2006)

Multivariate Empirical Orthogonal Function (EOF) analysis is a useful tool to study the EASM, given the complex space and time structures associated with the East Asian summer variability (Wang et al. 2008). Following Wang et al. (2008), Sun et al. (2010) identify two major modes of atmospheric circulation variability associated with the EASM by applying the MV-EOF analysis to boreal summer (June/July/August: JJA) mean anomalies of zonal and meridional winds at 850 and 200 hPa. Both of the two modes are linked to rainfall anomalies over East Asia. The first mode is very similar to the Pacific-Japan pattern (Nitta 1987; Kosaka and Nakamura 2006) and is associated with rainfall anomalies in the Meiyu/Changma/Baiu rain band while the second mode is associated with rainfall anomalies over northern China (Sun et al. 2010). These authors further found that the two EOF modes are both associated with ENSO during the previous winter (December/January/February: DJF; Sun et al. (2010)), implying that they can be partly reproduced, at least statistically, given the best possible information about tropical forcing. Furthermore, Ding et al. (2014) found that about 25 % of the variance of the first mode can be captured by a coupled climate model (the Kiel Climate Model, Park et al. (2009)) driven by observed wind stress anomalies alone. However, their coupled model fails to reproduce the variability of the second mode as seen in observations (Ding et al. 2014).

In this study, we revisit the two major modes (Sun et al. 2010) in an atmospheric general circulation model (GCM) coupled with a slab mixed layer model using a pacemaker technique similar to that described in Cash et al. (2010). We focus on how much skill the model can achieve at reproducing the variability of the two modes in ERA40. This is important according to the notion that the skill we find sets an upper limit of potential predictability in practice. Results show that the model can capture a significant part of the variability of both the first and second modes, which takes a step forward from Ding et al. (2014). In Section 2, the model and experiments are described. Section 3 presents the model results, and Section 4 provides a summary and conclusion.

2 Pacemaker experiments

In this study, the atmospheric model is the Geophysical Fluid Dynamics Laboratory AM2.1 (Global Atmospheric Model Development Team 2004; Delworth et al. 2006), which is coupled with a slab mixed layer model

of depth 50 m. To perform pacemaker experiments, the atmosphere/slab-ocean coupled model is first integrated with the ocean model temperature (model SST) restored to observed SST with a relaxation time scale of 1 day. In the integration, a quantity termed *q-flux* is calculated as the flux resulting from the restoring term. The *q-flux* represents the contribution of ocean dynamical processes, missing in the slab model, to SST evolution. In pacemaker experiments, the *q-flux* is added back to the coupled model as an external forcing. We emphasize that the *q-flux* added back to the pacemaker experiments is independent of the model state, so that ocean temperature in the model is not directly prescribed from the observations but, rather, is a fully prognostic quantity. Therefore, in pacemaker experiments, the atmosphere can both drive and be driven by ocean model temperature, avoiding some of the issues suffered by atmosphere-only or ocean-only simulations (see Greatbatch et al. (1995), Wang et al. (2005), Wu and Kirtman (2005), Wu et al. (2006), Wu and Kirtman (2007), and Griffies et al. (2009)). The pacemaker approach also has the advantage that the model climate is more constrained than in fully coupled models, avoiding some of the biases present in those models (Wang et al. 2014).

An ensemble of experiments is performed in which the monthly varying *q-flux* is prescribed in the central and eastern tropical Pacific (8° S–8° N, 172° E–the South American coast) while elsewhere the monthly climatological *q-flux* is prescribed. We stress that all the information about the time series of observed events comes from the *q-flux* that is applied in the central and eastern tropical Pacific corresponding to the region most strongly influenced by ENSO. The model is integrated from 1950 to 1999 with eight ensemble members differing only in their initial conditions. In this study, the ensemble mean of the eight integrations is analyzed and shown in the figures unless stated otherwise. The pacemaker experiments reproduce observed SST variability in the central and eastern tropical Pacific (not shown), as expected. These pacemaker experiments have been shown to capture a substantial part of the East Asian winter monsoon rainfall variability (Lu et al. 2011). Further information about the pacemaker experiments can be found in Lu et al. (2011).

3 Results

Like in Sun et al. (2010), we apply the same MV-EOF analysis to boreal summer (JJA) seasonal mean anomalies of ERA40 (Uppala et al. 2005) wind fields at 850 and 200 hPa. The domain of analysis covers 10° N–50° N and 100° E–150° E for the years 1958–2001. Prior to the EOF analysis, time series of interannual anomalies are calculated by removing the seasonal mean climatology, normalizing by

the spatially-averaged standard deviation and then weighting by the square root of cosine of latitude to provide equal

weighting of equal areas. The MV-EOF analysis method is described in detail in Wang (1992).

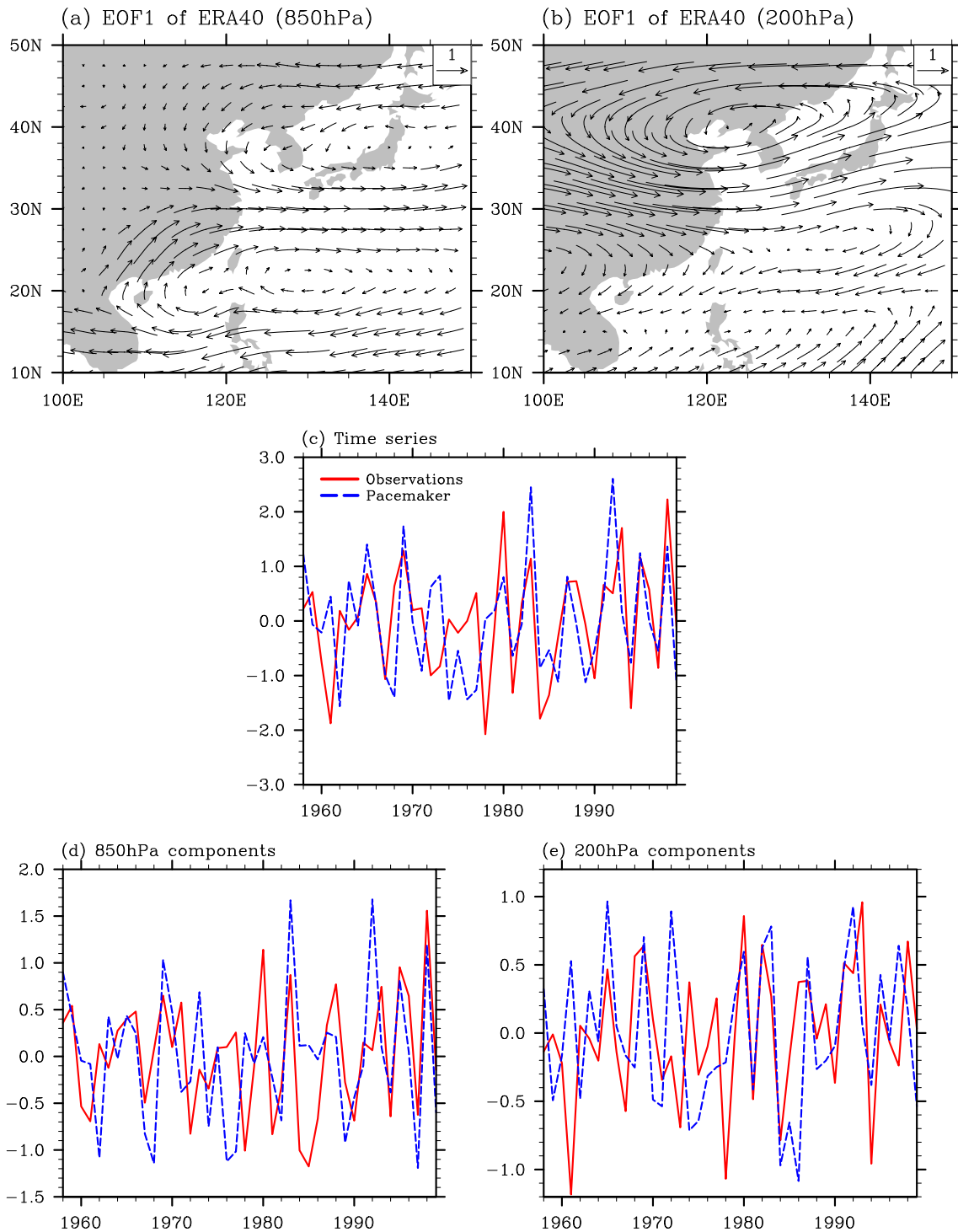


Fig. 1 Spatial patterns (a and b) of the first MV-EOF mode for 850 hPa winds (a) and 200 hPa winds (b) from ERA40. The corresponding time series from ERA40 (red line) and the pacemaker experiment (blue line), which are derived by projecting wind fields from the pacemaker experiment onto the spatial patterns of MV-EOF1 from ERA40, are shown in panel (c). The 850 hPa (d) and 200 hPa (e) components of the time series for ERA40 (red lines) and the

pacemaker experiment (blue lines) are derived by projecting wind fields only at 850 hPa (d) and only at 200 hPa (e) onto the spatial patterns at the corresponding levels for MV-EOF1 from ERA40. The first mode explains 20.6 % of variance in the ERA40 reanalysis. Note that the sample arrow in the top right hand corner has length corresponding to 1m s^{-1}

The spatial pattern (EOF) and associated principal component (PC) time series of the first mode, which explain

20.6 % of the variance, are shown in Fig. 1. Sun et al. (2010) noted that the positive phase of EOF1 at 850 hPa

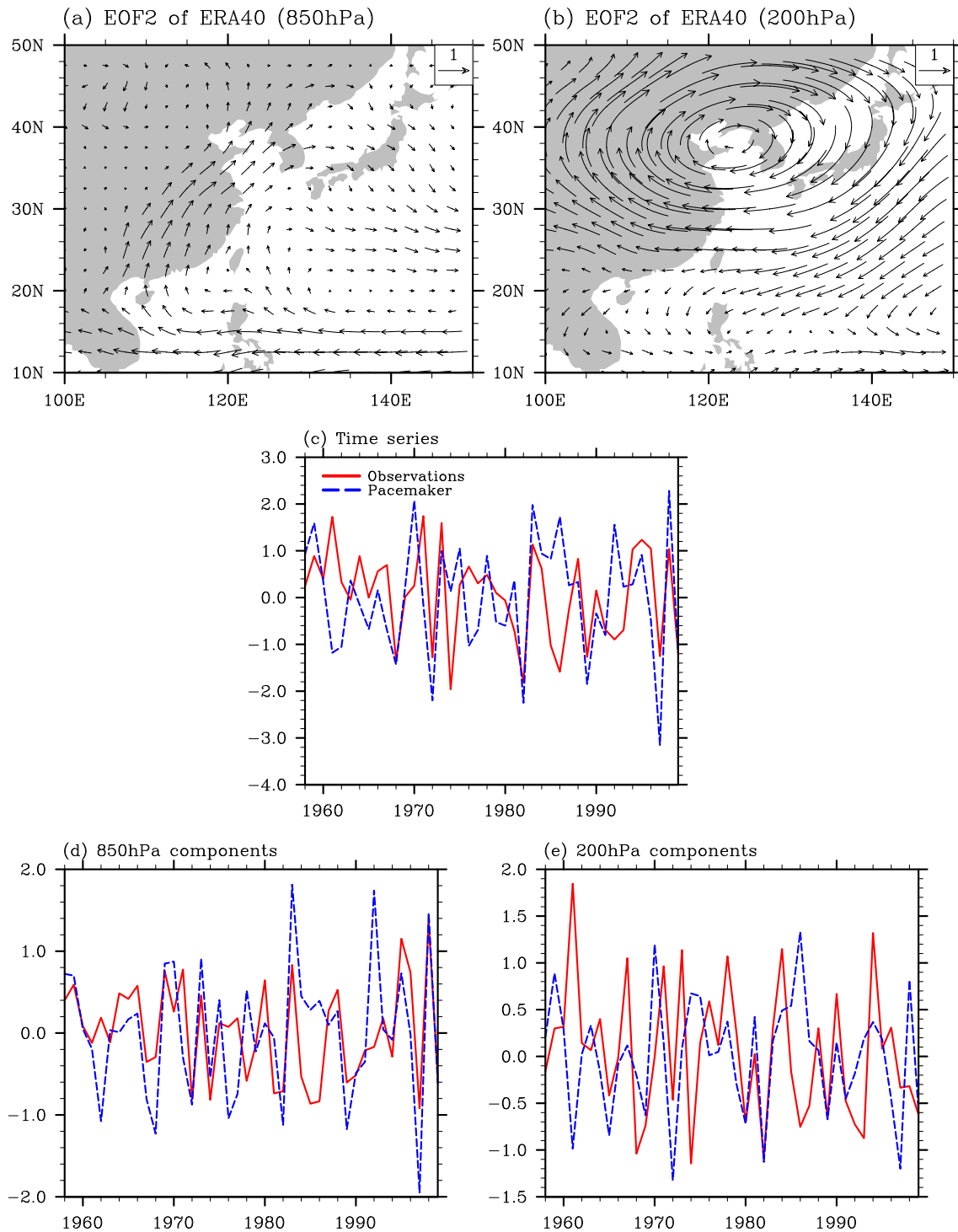


Fig. 2 Spatial patterns (**a** and **b**) of the second MV-EOF mode for 850 hPa winds (**a**) and 200 hPa winds (**b**) from ERA40. The corresponding time series from ERA40 (*red line*) and the pacemaker experiment (*blue line*), which are derived by projecting wind fields from the pacemaker experiment onto the spatial patterns of MV-EOF2 from ERA40, are shown in panel (**c**). The 850 hPa (**d**) and 200 hPa (**e**) components of the time series for ERA40 (*red lines*) and the

pacemaker experiment (*blue lines*) are derived by projecting wind fields only at 850 hPa (**d**) and only at 200 hPa (**e**) onto the spatial patterns at the corresponding levels for MV-EOF2 from ERA40. The second mode explains 12.1 % of variance in the ERA40 reanalysis. Note that the *sample arrow* in the top right hand corner has length corresponding to 1ms^{-1}

Table 1 Correlation coefficients between the time series from ERA40 and the pacemaker experiments for the two modes and their respective 850 and 200 hPa components in the three periods: 1958–1999, 1958–1978, and 1979–1999

	1958–1999	1958–1978	1979–1999
Mode 1	0.41*	−0.02	0.66*
850 hPa component	0.42*	0.15	0.58*
200 hPa component	0.31*	0.01	0.52*
Mode 2	0.37*	0.25	0.49*
850 hPa component	0.55*	0.47*	0.62*
200 hPa component	0.16	0.01	0.32

All the time series are detrended prior to calculating correlation. Correlations that are significantly different from zero at the 95 % level or higher (assuming each year to be independent) are shown with an *asterisk*

(Fig. 1a) resembles the negative phase of the Pacific-Japan (PJ) pattern (Nitta 1987; Kosaka and Nakamura 2006). At 200 hPa (Fig. 1b), the positive phase of EOF1 displays a large cyclonic anomaly associated with an anomalous westerly wind band between 30° N and 40° N (Sun et al. 2010). The anomalous westerly band is associated with a meridional shift of the East Asian Jet, of which the core is located between 40° N and 45° N (Lin and Lu 2005). The second mode, which explains 12.1 % of the variance, is shown in Fig. 2. The positive phase of EOF2 at 850 hPa is characterized by southerly wind anomalies extending northeastward and covering the southeastern part of China, Korea, and Japan (Fig. 2a). At 200 hPa, the positive phase of EOF2 features an anticyclonic anomaly (Fig. 2b). Recently, Greatbatch et al. (2013) argued that this mode is related to the variability of the Indian Summer Monsoon. As to the two modes, one can refer to Sun et al. (2010) for more details.

When assessing the pacemaker experiments, we project the model wind fields onto the corresponding spatial patterns of the two modes calculated from the ERA40 reanalysis. The resulting time series from the model are shown in Figs. 1c and 2c and compared to the corresponding time series from ERA40, respectively. To emphasize interannual variability, all time series are detrended prior to calculating correlations (in Table 1, one can find all the correlations between the model and ERA40); the plots, on the other hand, show the undetrended time series. Also, as a check, we have repeated the analysis by applying the MV-EOF analysis to the ensemble mean of the pacemaker experiments to calculate its own modes and corresponding PC time series. We find that the EOF modes from the ensemble mean of the pacemaker experiments (not shown) capture the main features seen in the modes from the ERA40 reanalysis. The correlations (not shown) between the PC time series corresponding to the main modes calculated from the ensemble mean of the pacemaker experiments and the PC time series from ERA40 are very little changed from those reported below. It should be noted, nevertheless, that we deliberately chose to project the model output onto the EOF

patterns derived from ERA-40 and not those obtained from the model ensemble mean. The reason is that given enough ensemble members, the ensemble mean contains only the forced response of the model to the imposed forcing, in this case to the ENSO forcing prescribed using the q-flux. The corresponding MVEOFs are not, therefore, guaranteed to correspond to those obtained from the ERA-40 reanalysis since the latter includes both a forced signal, e.g., from ENSO, plus internal variability.

Looking at Fig. 1c, it is apparent that the pacemaker experiments capture part of the variability of the first mode from ERA40, especially after 1979. The correlation between the two time series is 0.41 from 1958 to 1999, which is significantly different from zero at the 95 % confidence level, although there is effectively no correlation over the period 1958–1978 (see Table 1 and Ding et al. (2014) for further discussion of this issue). On the other hand, the correlation reaches 0.66 from 1979 to 1999, also statistically different from zero at the 95 % confidence level, when the influence of ENSO on the East Asia summer climate becomes stronger after the 1976/77 climate shift (e.g., Xie et al. 2010; Sun et al. 2010; Ding et al. 2014). It follows that about 40 % of the variability associated with the first mode is captured by the pacemaker experiments after 1979, which is greater than the 25 % reported by Ding et al. (2014). What is more interesting is that the pacemaker experiments also capture part of the variability of the second mode (Fig. 2c). The correlation is 0.37 from 1958 to 1999, which is lower than for the first mode, but still significantly different from zero at the 95 % confidence level. The pacemaker experiments also perform better for the second mode after 1979 with a higher correlation of 0.49—an important result given that no significant part of the second mode variability in ERA40 is captured in the previous work of Ding et al. (2014). Later, we will discuss possible reasons for success in the pacemaker experiments.

Lu et al. (2006) found that interannual variability of the lower troposphere summer circulation over the western North Pacific is dominated by tropical SST forcing, while

fluctuations of the upper troposphere circulation are dominated by atmospheric internal dynamics, independent of boundary forcings. Sun et al. (2010) found that a linear, dry dynamical model, when driven by the diabatic heating anomalies in the tropics associated with each mode, can reproduce many of the anomalous circulation features

for the lower troposphere, but not for the upper troposphere. These motivate us to investigate the lower and upper components of the two modes, separately.

To derive the contribution of the wind fields at 850 hPa to the time series (Figs. 1d and 2d), we project wind fields onto the corresponding spatial patterns of the two modes

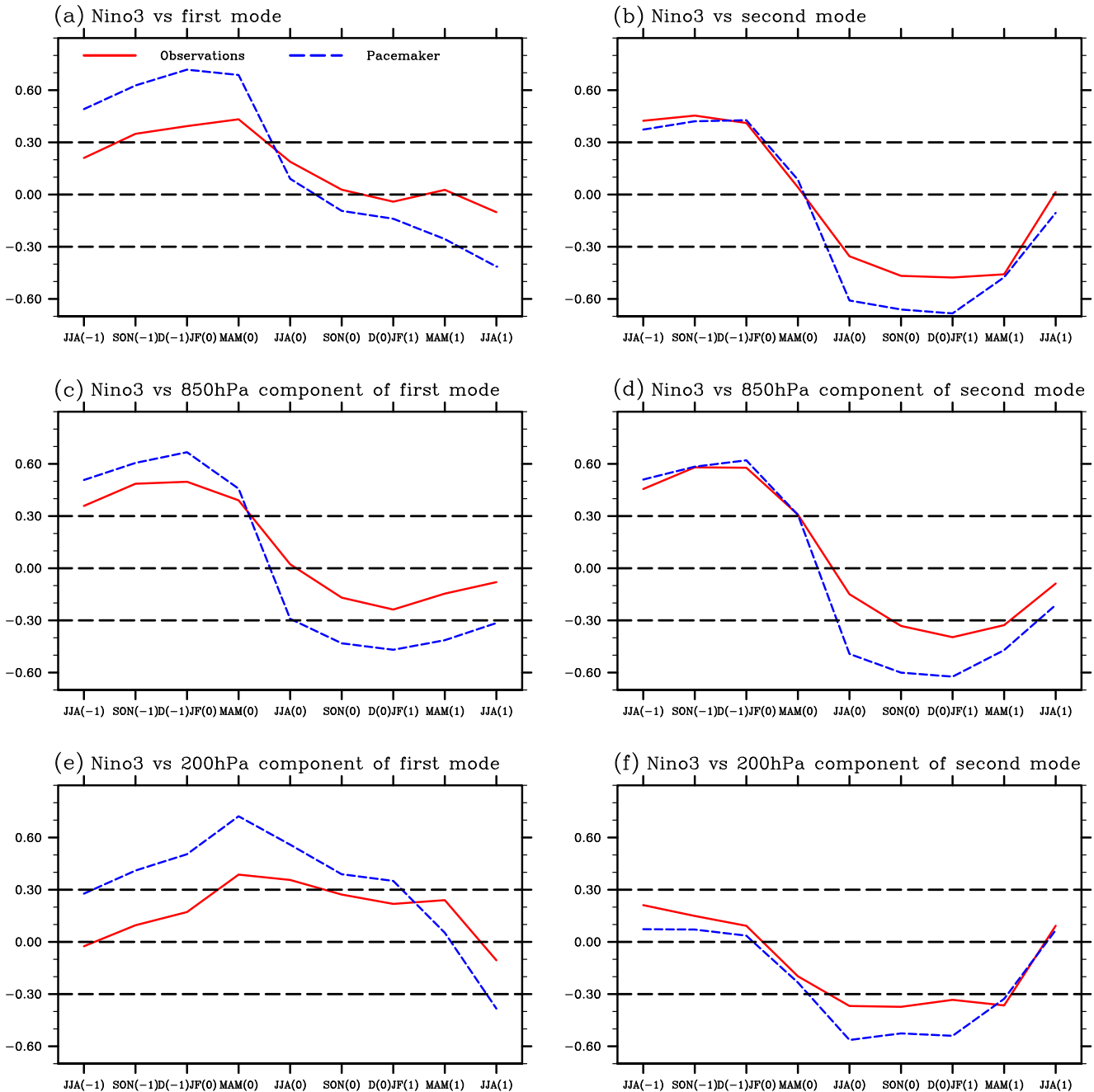


Fig. 3 Cross-correlation from the ensemble mean of the pacemaker experiments (shown in blue) between SST anomalies averaged over the Niño3 region (150° W–90° W, 5° S–5° N) from JJA(-1) to JJA(1) and time series over the period 1958–1999 for (a) the first mode; (b) the second mode; (c) the 850 hPa component of the first mode; (d) the 850 hPa component of the second mode; (e) the 200 hPa component of the first mode; and (f) the 200 hPa component of the second mode. For

observations (shown in red), the time series are calculated from the ERA40 reanalysis (Uppala et al. 2005) and Niño3 SST anomalies are calculated from the HadISST1.1 (Rayner et al. 2003). Note that (0) indicates the summer simultaneous with the MV-EOF analysis, -1 indicates the preceding year and 1 the following year. The three horizontal black dashed lines represent the 95 % confidence level based on a Student's *t* test and the zero line, respectively

only at 850 hPa. Likewise, we can also derive the contribution of wind fields at 200 hPa to the time series (Figs. 1e and 2e) by projecting wind fields onto the spatial pattern of the two modes only at 200 hPa. The pacemaker experiments perform well for both the 850 hPa and the 200 hPa components of the first mode when looking at the whole period 1958–1999 and also the subperiod 1979–1999. The correlations between the model and ERA40 from 1958 to 1999 are 0.42 and 0.31 (both statistically different from zero at the 95 % confidence level) for 850 and 200 hPa, respectively (see Table 1). As we found using projection onto the full EOF pattern at both 850 and 200 hPa, the correlation is only significant after 1979, this being true for both the lower (0.58) and upper (0.52) components, and with effectively no correlation over the period 1958–1978. It follows that about 25 % variance of the 200 hPa component of the first mode is captured by the pacemaker experiments after 1979, which is an important result given that interannual variability of the upper tropospheric circulation is thought to be dominated by internal atmospheric dynamics (Lu et al. 2006). Different from the first mode, the pacemaker experiment performs well only at 850 hPa for the second mode. The correlation between the model and ERA40 is 0.55 from 1958 to 1999 for the 850 hPa component (Fig. 2d), but only 0.16 for the 200 hPa component (Fig. 2e). Also, in contrast to the first mode, the model performs well for the 850 hPa component in both time periods 1958–1978 and 1979–1999.

We now turn to discussion of the relationship between the EASM and ENSO. It has been noted that both the modes are associated with the declining phase of ENSO in observations (Wang et al. 2008; Sun et al. 2010). Ding et al. (2014) argue that reproducing the link between the first mode and ENSO enables their model to capture part of the variability of the first mode. Figure 3 shows the cross-correlation between the time series for each mode and SST anomalies averaged over the Niño3 region for observations and the model, respectively. It is apparent that the relationships

between the two modes and ENSO seen in observations are captured by the pacemaker experiments (Fig. 3a and b). For instance, the pacemaker experiments reproduce the link of the first mode to the decaying phase of ENSO seen in observations even though the correlation is higher in the model (Fig. 3a). What is surprising is that in the pacemaker experiments, the second mode is linked with both the decaying and the developing phase of ENSO, like in observations (Fig. 3b). We argue that the success in capturing a substantial amount of variance of both the modes in ERA40 must be due to being able to capture the delayed impact of ENSO on the EASM in the model, given that SST forcing in the central and eastern tropical Pacific is the only information in the model about the time series of events in the real world.

We have also investigated the relationship between ENSO and the respective 850 and 200 hPa components of the two modes (Fig. 3c, d, e, and f). For the first mode, the 850 hPa component is significantly correlated with Niño3 SST variability in the previous winter whereas the 200 hPa component is linked with Niño3 SST variability in the previous spring. For the second mode, the 850 hPa component is also significantly correlated with Niño3 SST variability in the previous winter but there is no significant relationship when ENSO leads the 200 hPa component. These results are consistent with the reproducibility of the 850 and 200 hPa components of the modes noted earlier and add strength to the argument that the success of the pacemaker experiments at capturing part of the variability of the EASM comes from their ability to capture the ENSO/EASM relationship.

The relationship between ENSO and the EASM (with ENSO leading), as revealed by ERA-40 and HadISST data sets for the two periods 1958–1978 and 1979–1999, is further illustrated in Table 2. It is clear that the link for both strengthens after 1979, especially for the first mode for which there is no significant link before 1979, as noted

Table 2 Correlation coefficients between Niño3 SST variability in the previous winter and the two modes and their respective 850 and 200 hPa components in the three periods: 1958–1999, 1958–1978, and 1979–1999, except for the 200 hPa component of the first mode which is correlated with Niño3 SST variability in the previous spring

	1958–1999	1958–1978	1979–1999
Mode 1	0.39*	−0.06	0.63*
850 hPa component	0.50*	0.11	0.71*
200 hPa component	0.39*	0.13	0.45*
Mode 2	0.41*	0.37	0.52*
850 hPa component	0.58*	0.39	0.74*
200 hPa component	0.09	0.21	0.01

All the time series are detrended prior to calculating correlation. Correlations that are significantly different from zero at the 95 % level or higher (assuming each year to be independent) are shown with an asterisk. Here, time series for the two modes and their respective 850 and 200 hPa components are calculated from the ERA40 reanalysis (Uppala et al. 2005) and Niño3 SST anomalies are calculated from the HadISST1.1 (Rayner et al. 2003)

earlier (see also Ding et al. (2014)). In particular, the correlation coefficients between the first (second) mode and ENSO in the previous winter are -0.06 (0.37) and 0.63 (0.52) for 1958–1978 and 1979–1999, respectively. The stronger link to ENSO after 1979 can also be seen for the 850 hPa component of the first (second) mode with correlation coefficients of 0.11 (0.39) and 0.71 (0.74) for 1958–1978 and 1979–1999, respectively. The strong similarity between the correlation coefficients shown in Tables 1 and 2 provides strong evidence of the ability of the pacemaker experiments to capture the observed ENSO/EASM relationship (with ENSO leading), noting that in the pacemaker experiments the only interannual forcing comes from ENSO.

Finally, we note that the correlation between Nino3 SST anomalies and the first mode and its 850 and 200 hPa components are much higher for the experiments than in the observations. A possible reason is that the correlations shown for the experiments are for the ensemble mean, filtering out the noise and increasing the signal (here ENSO-forced) to noise ratio. We have also calculated the cross-correlation for the individual ensemble members and find that they still capture the delayed impact of ENSO on the EASM even though the correlation coefficients are lower (not shown).

4 Summary and conclusion

In this study, we have revisited the two major modes of variability of the East Asian Summer Monsoon (EASM) identified by Sun et al. (2010) using the pacemaker experiments of Lu et al. (2011). In the pacemaker experiments, all the information about the time series of events in the real world comes from the *q-flux* that is applied in the central and eastern tropical Pacific. The advantage of the pacemaker experiments is that SST is a fully prognostic variable and can freely interact with the atmospheric model (Cash et al. 2010; Lu et al. 2011), avoiding some of the issues inherent in atmosphere-only or ocean-only simulations (Greatbatch et al. 1995; Wang et al. 2005; Wu and Kirtman 2005; Wu et al. 2006; Wu and Kirtman 2007; Griffies et al. 2009).

The two modes are calculated by applying a MV-EOF analysis to boreal summer (June/July/August) seasonal mean anomalies of the zonal and meridional winds in the lower (850 hPa) and the upper (200 hPa) troposphere from the ERA40 reanalysis (Uppala et al. 2005), and corresponding principal components (PC) measure the variability of the modes. For the pacemaker experiments, we project the model wind fields onto the respective spatial patterns of the two modes from the ERA40 reanalysis to derive the corresponding time series. Results indicate that the model

can capture a significant part of the variability of both the first and second modes. The correlation coefficients using detrended time series between the pacemaker experiments and ERA40 from 1958 to 1999 are 0.41 and 0.37 for the first and second modes, respectively. These correlation coefficients increase to 0.66 and 0.49 after 1979, consistent with stronger ENSO forcing after the 1976/1977 climate shift (e.g., Xie et al. 2010). The results from the pacemaker experiments take a step forward from Ding et al. (2014). In particular, the pacemaker experiments can capture about 25 % of variance of the second mode after 1979. We argue that the key element is to capture the delayed impact of ENSO on the East Asian summer climate, something that is still a challenge for many of the state-of-the-art coupled models that took part in CMIP5 (Fu et al. 2013). Indeed, the close agreement between the correlation coefficients in Tables 1 and 2 is a tribute to the ability of the pacemaker experiments to capture this relationship.

We also investigate the respective 850 and 200 hPa components of the two modes. To derive the 850 hPa (200 hPa) components, we project wind fields from only 850 hPa (200 hPa) onto the corresponding spatial patterns of the two modes. For the first mode, the 850 and 200 hPa components are almost equally well captured by the pacemaker experiments whereas for the second mode, only the 850 hPa component can be captured.

Finally, we note that the MVEOF analysis used here is not dependent on the use of the ERA-40 reanalysis. Wang et al. (2008) originally obtained the same two MVEOFs using a version of the NCEP reanalysis (Kanamitsu et al. 2002) and, as noted in Section 3, the same two MVEOFs emerge when the analysis is applied to the ensemble mean of the pacemaker experiments. Another example is given in Figs. 5 and 6 of Ding et al. (2014). We have also repeated the complete analysis carried out in this paper using both the NCEP and ERA-Interim reanalysis and found little change to the results (not shown).

Acknowledgments HD and RJG are grateful for continued support from GEOMAR. JL is supported by the Office of Science of the U.S. Department of Energy as part of the Regional and Global Climate Modeling program. BC acknowledges the support from the National Science Foundation (grants 0830068, 0957884, and 1338427), National Oceanic and Atmospheric Administration (grant NA09OAR4310058), and National Aeronautics and Space Administration (grant NNX09AN50G). We are grateful to two anonymous reviewers for their helpful comments.

References

- Cash BA, Rodó X, Kinter III JL, Yunus M (2010) Disentangling the impact of ENSO and Indian ocean variability on the regional climate of Bangladesh: Implications for cholera risk. *J Climate* 23(10):2817–2831. doi:10.1175/2009JCLI2512.1

- Delworth TL, Broccoli AJ, Rosati A, Stouffer RJ, Balaji V, Beesley JA, Cooke WF, Dixon KW, Dunne J, Dunne K et al (2006) GFDL's CM2 global coupled climate models. Part I: Formulation and simulation characteristics. *J Climate* 19(5):643–674. doi:[10.1175/JCLI3629.1](https://doi.org/10.1175/JCLI3629.1)
- Ding H, Greatbatch RJ, Park W, Latif M, Semenov VA, Sun X (2014) The variability of the East Asian summer monsoon and its relationship to ENSO in a partially coupled climate model. *Climate Dyn* 40(1):367–379. doi:[10.1007/s00382-012-1642-3](https://doi.org/10.1007/s00382-012-1642-3)
- Fu Y, Lu R, Wang H, Yang X (2013) Impact of overestimated ENSO variability in the relationship between ENSO and East Asian summer rainfall. *J Geophys Res* 118(12):6200–6211. doi:[10.1002/jgrd.50482](https://doi.org/10.1002/jgrd.50482)
- Global Atmospheric Model Development Team (2004) The New GFDL Global Atmosphere and Land Model AM2/LM2: Evaluation with Prescribed SST Simulations. *J Climate* 17(17):4641–467. doi:[10.1175/JCLI3223.1](https://doi.org/10.1175/JCLI3223.1)
- Greatbatch RJ, Li G, Zhang S (1995) Hindcasting ocean climate variability using time-dependent surface data to drive a model: an idealized study. *J Phys Oceanogr* 25(11):2715–2725. doi:[10.1175/1520-0485\(1995\)025<2715:HOCVUT>2.0.CO;2](https://doi.org/10.1175/1520-0485(1995)025<2715:HOCVUT>2.0.CO;2)
- Greatbatch RJ, Sun X, Yang XQ (2013) Impact of variability in the Indian summer monsoon on the East Asian summer monsoon. *Atmosph Sci Lett* 14(1):14–19. doi:[10.1002/asl2.408](https://doi.org/10.1002/asl2.408)
- Griffies S, Biastoch A, Böning C, Bryan F, Danabasoglu G, Chassignet E, England M, Gerdes R, Haak H, Hallberg R et al (2009) Coordinated ocean-ice reference experiments (COREs). *Ocean Model* 26(1–2):1–46. doi:[10.1016/j.ocemod.2008.08.007](https://doi.org/10.1016/j.ocemod.2008.08.007)
- Kanamitsu M, Ebisuzaki W, Woollen J, Yang SK, Hnilo J, Fiorino M, Potter G (2002) NCEP-DOE AMIP-II Reanalysis (R-2). *Bull Am Meteorol Soc* 83(11):1631–1643. doi:[10.1175/BAMS-83-11-1631](https://doi.org/10.1175/BAMS-83-11-1631)
- Kosaka Y, Nakamura H (2006) Structure and dynamics of the summertime Pacific–Japan teleconnection pattern. *Quart J Roy Meteor Soc* 132(619):2009–2030. doi:[10.1256/qj.05.204](https://doi.org/10.1256/qj.05.204)
- Lau NC, Nath MJ (2006) ENSO modulation of the interannual and intraseasonal variability of the East Asian monsoon-A model study. *J Climate* 19(18):4508–4530. doi:[10.1175/JCLI3878.1](https://doi.org/10.1175/JCLI3878.1)
- Li C, Lu R, Dong B (2012) Predictability of the western North Pacific summer climate demonstrated by the coupled models of ENSEMBLES. *Climate Dyn* 39(1–2):2. doi:[10.1007/s00382-011-1274-z](https://doi.org/10.1007/s00382-011-1274-z)
- Li C, Lu R, Dong B (2014) Predictability of the western North Pacific summer climate associated with different ENSO phases by ENSEMBLES multi-model seasonal forecasts. *Climate Dyn* 43(11–12):1829–1845. doi:[10.1007/s00382-013-2010-7](https://doi.org/10.1007/s00382-013-2010-7)
- Li Y, Lu R, Dong B (2007) The ENSO-Asian monsoon interaction in a coupled ocean-atmosphere GCM. *J Climate* 20(20):5164–5177. doi:[10.1175/JCLI4289.1](https://doi.org/10.1175/JCLI4289.1)
- Lin Z, Lu R (2005) Interannual meridional displacement of the East Asian upper-tropospheric jet stream in summer. *Adv Atmos Sci* 22(2):199–211. doi:[10.1007/BF02918509](https://doi.org/10.1007/BF02918509)
- Lu J, Zhang M, Cash B, Li S (2011) Oceanic forcing for the East Asian precipitation in pacemaker AGCM experiments. *Geophys Res Lett* 38(12):12,702. doi:[10.1029/2011GL047614](https://doi.org/10.1029/2011GL047614)
- Lu R, Li Y, Dong B (2006) External and internal summer atmospheric variability in the Western North Pacific and East Asia. *J Meteor Soc Japan* 84(3):447–462
- Nitta T (1987) Convective activities in the tropical western Pacific and their impact on the Northern Hemisphere summer circulation. *J Meteor Soc Japan* 65(3):373–390
- Park W, Keenlyside N, Latif M, Ströh A, Redler R, Roeckner E, Madec G (2009) Tropical Pacific climate and its response to global warming in the Kiel Climate Model. *J Climate* 22(1):71–92. doi:[10.1175/2008JCLI2261.1](https://doi.org/10.1175/2008JCLI2261.1)
- Philander S (1990) *El Niño, La Niña, and the southern oscillation*. Academic Press
- Rayner N, Parker D, Horton E, Folland C, Alexander L, Rowell D, Kent E, Kaplan A (2003) Global analyses of sea surface temperature, sea ice, and night marine air temperature since the late nineteenth century. *J Geophys Res* 108(D14):4407–4453. doi:[10.1029/2002JD002670](https://doi.org/10.1029/2002JD002670)
- Rodwell M, Hoskins B (2001) Subtropical anticyclones and summer monsoons. *J Climate* 14(15):3192–3211. doi:[10.1175/1520-0442\(2001\)014<3192:SAASM>2.0.CO;2](https://doi.org/10.1175/1520-0442(2001)014<3192:SAASM>2.0.CO;2)
- Sun X, Greatbatch RJ, Latif M (2010) Two major modes of variability of the East Asian summer monsoon. *Quart J Roy Meteor Soc* 136(649):829–841. doi:[10.1002/qj.635](https://doi.org/10.1002/qj.635)
- Uppala S, Kållberg P, Simmons A, Andrae U, Bechtold V, Fiorino M, Gibson J, Haseler J, Hernandez A, Kelly G et al (2005) The ERA-40 re-analysis. *Quart J Roy Meteor Soc* 131(612):2961–3012. doi:[10.1256/qj.04.176](https://doi.org/10.1256/qj.04.176)
- Wang B (1992) The vertical structure and development of the ENSO anomaly mode during 1979–1989. *J Atmos Sci* 49(8):698–712. doi:[10.1175/1520-0469\(1992\)049<0698:TVSADO>2.0.CO;2](https://doi.org/10.1175/1520-0469(1992)049<0698:TVSADO>2.0.CO;2)
- Wang B, Ding Q, Fu X, Kang I, Jin K, Shukla J, Doblas-Reyes F (2005) Fundamental challenge in simulation and prediction of summer monsoon rainfall. *Geophys Res Lett* 32(15):L15,711. doi:[10.1029/2005GL022734](https://doi.org/10.1029/2005GL022734)
- Wang B, Wu R, Fu X (2000) Pacific-east Asian teleconnection: How does ENSO affect east Asian climate? *J Climate* 13(9):1517–1536. doi:[10.1175/1520-0442\(2000\)013<1517:PEATHD>2.0.CO;2](https://doi.org/10.1175/1520-0442(2000)013<1517:PEATHD>2.0.CO;2)
- Wang B, Wu Z, Li J, Liu J, Chang C, Ding Y, Wu G (2008) How to measure the strength of the East Asian summer monsoon. *J Climate* 21(17):4449–4463. doi:[10.1175/2008JCLI2183.1](https://doi.org/10.1175/2008JCLI2183.1)
- Wang B, Zhang Q (2002) Pacific-East Asian Teleconnection. Part II: How the Philippine Sea Anomalous Anticyclone is Established during El Niño Development. *J Climate* 15(22):3252–3265. doi:[10.1175/1520-0442\(2002\)015<3252:PEATPI>2.0.CO;2](https://doi.org/10.1175/1520-0442(2002)015<3252:PEATPI>2.0.CO;2)
- Wang C, Zhang L, Lee SK, Wu L, Mechoso CR (2014) A global perspective on CMIP5 climate model biases. *Nat Clim Change* 4(3):201–205. doi:[10.1038/nclimate2118](https://doi.org/10.1038/nclimate2118)
- Wu R, Hu Z, Kirtman B (2003) Evolution of ENSO-related rainfall anomalies in East Asia. *J Climate* 16(22):3742–3758. doi:[10.1175/1520-0442\(2003\)016<3742:EOERAI>2.0.CO;2](https://doi.org/10.1175/1520-0442(2003)016<3742:EOERAI>2.0.CO;2)
- Wu R, Kirtman B (2004) Impacts of the Indian Ocean on the Indian summer monsoon-ENSO relationship. *J Climate* 17(15):3037–3054. doi:[10.1175/1520-0442\(2004\)017<3037:LOTIOO>2.0.CO;2](https://doi.org/10.1175/1520-0442(2004)017<3037:LOTIOO>2.0.CO;2)
- Wu R, Kirtman B (2005) Roles of Indian and Pacific Ocean air–sea coupling in tropical atmospheric variability. *Climate Dyn* 25(2):155–170. doi:[10.1007/s00382-005-0003-x](https://doi.org/10.1007/s00382-005-0003-x)
- Wu R, Kirtman B (2007) Regimes of seasonal air–sea interaction and implications for performance of forced simulations. *Climate Dyn* 29(4):393–410. doi:[10.1007/s00382-007-0246-9](https://doi.org/10.1007/s00382-007-0246-9)
- Wu R, Kirtman B, Pegion K (2006) Local air–sea relationship in observations and model simulations. *J Climate* 19(19):4914–4932. doi:[10.1175/JCLI3904.1](https://doi.org/10.1175/JCLI3904.1)
- Xie S, Du Y, Huang G, Zheng X, Tokinaga H, Hu K, Liu Q (2010) Decadal Shift in El Niño Influences on Indo-Western Pacific and East Asian Climate in the 1970s. *J Climate* 23(12):3352–3368. doi:[10.1175/2010JCLI3429.1](https://doi.org/10.1175/2010JCLI3429.1)
- Xie SP, Hu K, Hafner J, Tokinaga H, Du Y, Huang G, Sampe T (2009) Indian Ocean capacitor effect on Indo-western Pacific climate during the summer following El Niño. *J Climate* 22(3):730–747. doi:[10.1175/2008JCLI2544.1](https://doi.org/10.1175/2008JCLI2544.1)
- Zhang R, Sumi A, Kimoto M (1999) A diagnostic study of the impact of El Niño on the precipitation in China. *Adv Atmos Sci* 16(2):229–241. doi:[10.1007/BF02973084](https://doi.org/10.1007/BF02973084)